JCI insight

Alteration of myocardial GRK2 produces a global metabolic phenotype

Benjamin P. Woodall, … , Konstantinos Drosatos, Walter J. Koch

JCI Insight. 2019;4(10):e123848. https://doi.org/10.1172/jci.insight.123848.

Research Article | Cell biology | Metabolism

A vast body of literature has established G protein–coupled receptor kinase 2 (GRK2; family: β-adrenergic receptor kinases [βARKs]) as a key player in the development and progression of heart failure. Inhibition of GRK2 improves cardiac function after injury in numerous animal models. In recent years, discovery of several noncanonical GRK2 targets has expanded our view of this kinase. This article describes the exciting finding that cardiac GRK2 activity can regulate whole-body metabolism. Transgenic mice with cardiac-specific expression of a peptide inhibitor of GRK2 (TgβARKct) display an enhanced obesogenic phenotype when fed a high-fat diet (HFD). In contrast, mice with cardiac-specific overexpression of GRK2 (TgGRK2) show resistance to HFD-induced obesity. White adipose tissue (WAT) mass was significantly enhanced in HFD-fed TgβARKct mice. Furthermore, regulators of adipose differentiation were differentially regulated in WAT from mice with gain or loss of GRK2 function. Using complex metabolomics, we found that cardiac GRK2 signaling altered myocardial branched-chain amino acid (BCAA) and endocannabinoid metabolism. In addition, it modulated circulating BCAA and endocannabinoid metabolite profiles on mice fed an HFD. We also found that one of the BCAA metabolites identified here enhances adipocyte differentiation in vitro. These results suggest that metabolic changes in the heart due to GRK2 signaling on mice fed an HFD control whole-body metabolism.

JCI insight

RESEARCH ARTICLE

Alteration of myocardial GRK2 produces a global metabolic phenotype

Benjamin P. Woodall, Kenneth S. Gresham, Meryl A. Woodall, Mesele-Christina Valenti, Alessandro Cannavo, Jessica Pfleger, J. Kurt Chuprun, Konstantinos Drosatos, and Walter J. Koch

Center for Translational Medicine and Department of Pharmacology, Lewis Katz School of Medicine, Temple University, Philadelphia, Pennsylvania, USA.

A vast body of literature has established G protein–coupled receptor kinase 2 (GRK2; family: β-adrenergic receptor kinases [βARKs]) as a key player in the development and progression of heart failure. Inhibition of GRK2 improves cardiac function after injury in numerous animal models. In recent years, discovery of several noncanonical GRK2 targets has expanded our view of this kinase. This article describes the exciting finding that cardiac GRK2 activity can regulate whole-body metabolism. Transgenic mice with cardiac-specific expression of a peptide inhibitor of GRK2 (TgβARKct) display an enhanced obesogenic phenotype when fed a high-fat diet (HFD). In contrast, mice with cardiac-specific overexpression of GRK2 (TgGRK2) show resistance to HFD-induced obesity. White adipose tissue (WAT) mass was significantly enhanced in HFD-fed TgβARKct mice. Furthermore, regulators of adipose differentiation were differentially regulated in WAT from mice with gain or loss of GRK2 function. Using complex metabolomics, we found that cardiac GRK2 signaling altered myocardial branched-chain amino acid (BCAA) and endocannabinoid metabolism. In addition, it modulated circulating BCAA and endocannabinoid metabolite profiles on mice fed an HFD. We also found that one of the BCAA metabolites identified here enhances adipocyte differentiation in vitro. These results suggest that metabolic changes in the heart due to GRK2 signaling on mice fed an HFD control whole-body metabolism.

Introduction

The global prevalence of obesity has reached epidemic proportions. Obesity is a multiorgan disorder, which over time predisposes individuals to numerous comorbidities including hyperlipidemia, type II diabetes, hypertension, stroke, myocardial infarction, and heart failure (1, 2). In the majority of cases, lifestyle modifications and weight loss are successful only in the short term, with roughly 95% of individuals unable to sustain these changes beyond 3 years (3). Thus, a deeper understanding of mechanisms that govern metabolic regulation is required to develop effective therapeutic strategies.

In recent years, a number of studies have identified mechanisms of crosstalk between metabolic tissues to modulate energy expenditure. Peroxisome proliferator-activated receptor gamma coactivator 1-alpha–dependent expression and irisin secretion from the skeletal muscle can induce browning of white adipose tissue (WAT), promoting energy expenditure and resistance to obesity (4). Other studies have shown a communicative link between the liver, muscle, and adipose tissue as a way to control metabolic homeostasis (5, 6). Studies from the Olson lab describe a key role for the heart in systemic metabolic control (7, 8). Cardiac-specific overexpression of Mediator Complex Subunit 13 (MED13), a subunit of the Mediator complex, confers resistance to HFD-induced obesity and insulin resistance in mice (7). Increased mitochondrial content and lipid oxidation in both the liver and WAT directly contribute to the lean phenotype of MED13 cardiac transgenic mice, providing clear evidence of a communicative link between the heart and distant tissues for the purpose of systemic energy homeostasis (8).

Desensitization of activated β-adrenergic receptors (βARs) by G protein–coupled receptor kinases (GRKs) is an essential part of normal heart function. During heart failure (HF) however, sympathetic overdrive generates a maladaptive increase in GRK2 expression and activity in the heart, resulting in loss of βAR density and inotropic reserve (9–11). Inhibition of GRK2 using βARKct (a C-terminal peptide that competes with GRK2 binding to $G_{\beta\gamma}$) prevents and even reverses HF in several models (12–18). Importantly, in recent years, several groups have identified novel, noncanonical signaling roles for GRK2 involving targets other

Conflict of interest: The authors have declared that no conflict of interest exists.

Submitted: July 30, 2018
Accepted: April 2, 2019
Published: May 16, 2019.

Reference information: *JCI Insight*. 2019;4(10):e123848. https://doi.org/10.1172/jci.insight.123848.

than G protein–coupled receptors (GPCRs). Our own lab has found GRK2 to localize at the cardiomyocyte mitochondria where it alters respiration and plays an active role in mitochondria-mediated death pathways (19, 20). GRK2 has also been identified as a regulator of insulin signaling, promoting insulin resistance in the heart by phosphorylation of insulin receptor substrate-1 (21). Furthermore, systemic downregulation of GRK2 in hemizygous mice is protective in models of insulin resistance (22). Interestingly, these mice show modest resistance to weight gain when placed on an HFD (22). Likewise, inducible global GRK2 knockdown after 8 weeks of HFD improves insulin signaling and halts further weight gain in mice (23).

Due to these data, metabolic regulation by GRK2 clearly warrants further examination. In this study, we sought to better characterize the metabolic roles of GRK2 in the hearts of mice challenged with HFD. We report surprising metabolic phenotypes that arise from modulation of GRK2 activity exclusively in the heart. We show that transgenic βARKct (TgβARKct) mice (cardiac-specific expression of GRK2 inhibitory peptide) are more susceptible to HFD-induced obesity. TgβARKct mice exhibit a marked increase in adiposity on HFD relative to control animals. Conversely, transgenic GRK2 mice (TgGRK2) (cardiac-specific overexpression of GRK2) show resistance to weight gain on an HFD and a decrease in adipose tissue mass relative to control animals. Furthermore, one of the BCAA metabolites that is increased in serum and myocardial samples of TgβARKct mice enhances adipocyte differentiation in vitro. These results suggest that changes in cardiac metabolism on an HFD due to GRK2 signaling in the heart alters circulating metabolite profiles to control whole-body metabolism targeting primarily adiposity.

Results

TgβARKct mice are more susceptible to HFD-induced obesity. Previous research from our lab identified a direct correlation between GRK2 activity levels and insulin signaling in the heart (21). To continue these studies, we decided to examine the effect of cardiac GRK2 inhibition on HFD-induced insulin resistance and the development of diabetic cardiomyopathy. We found the surprising data that TgβARKct mice are more susceptible to HFD-induced weight gain compared with obesity found after HFD in nontransgenic littermate control (NLC) mice (Figure 1, A and B, and Supplemental Figure 2A; supplemental material available online with this article; https://doi.org/10.1172/jci.insight.123848DS1). TgβARKct mice fed an HFD increased their body weight by 66% within 6 weeks, whereas NLC mice gained only 44% body weight during the same period. These results are particularly striking in light of the fact that βARKct transgene expression is exclusive to the cardiac myocyte in these mice (Supplemental Figure 1A). Interestingly, this metabolic phenotype only becomes apparent with HFD, as we observe no difference in weight gain between TgβARKct and NLC mice during 6 weeks on a control diet (CD) (Figure 1, A and B).

Postmortem examination of the mice revealed that the enhanced weight gain in TgβARKct animals fed an HFD was, at least in part, due to an increase in adipose mass. Visceral white adipose fat pads were significantly larger in HFD-fed TgβARKct mice compared with NLC (Figure 1, C and D). In agreement with body weight data, we find this phenotype to be HFD dependent, with no baseline difference in adipose tissue weight between TgβARKct and NLC mice fed a CD (Figure 1, C and D).

Histological analysis of epididymal WAT (eWAT) revealed significant adipocyte hypertrophy in HFD-fed TgβARKct mice relative to the NLC group (Figure 1, E and F). In addition, we observed a significant increase in subscapular brown adipose tissue (BAT) mass of TgβARKct mice fed an HFD relative to TgβARKct animals fed a CD, whereas no such increase was seen in NLC mice (Figure 2B). Similarly, BAT histology demonstrates significant ectopic lipid deposition and adipocyte hypertrophy in the HFD-fed TgβARKct mice, with overall morphological characteristics more in line with that of WAT (Figure 2A). By contrast, the BAT morphology of NLC animals fed an HFD appears relatively normal, with smaller adipocytes and less evidence of ectopic lipid storage. Increased weight gain in TgβARKct animals was not caused by differences in systemic respiration or physical activity, as measured by metabolic cages (Supplemental Figure 3, A–F).

We did not detect an increase in the levels of serum triglycerides in either TgβARKct or NLC mice fed an HFD (Figure 2C). However, triglyceride levels in liver tissue were significantly elevated in HFD-fed TgβARKct mice compared with NLCs (Figure 2D). This result is consistent with the obese phenotype of the TgβARKct mice, reflecting a higher body lipid content in these mice and indicates ectopic deposition of lipids in nonadipose tissues. Interestingly, although not statistically significant, liver triglyceride levels trended lower in TgβARKct mice compared with NLC mice when maintained on the CD.

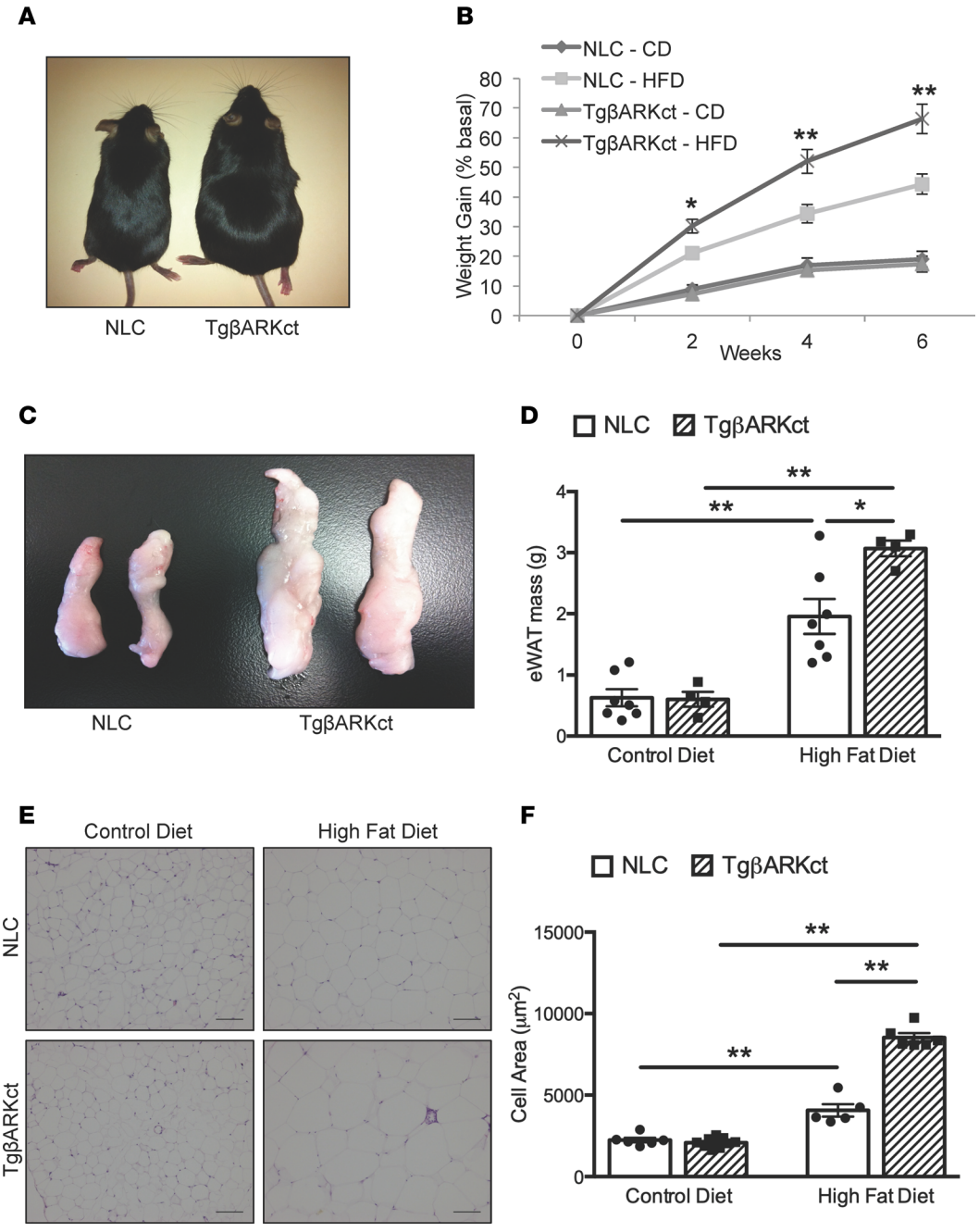

Figure 1. TgβARKct mice display an enhanced obesogenic phenotype following HFD. (**A**) TgβARKct and NLC mice after 6 weeks of HFD compared to same genotypes fed a CD. (**B**) Percentage weight gain of TgβARKct and NLC mice fed CD or HFD for 6 weeks. n = 7–16 per group; $^{*}P < 0.05$; $^{**}P < 0.01$. (**C**) Representative gross images of eWAT from TgβARKct and NLC mice fed CD or HFD. (**D**) Mass of eWAT isolated from TgβARKct and NLC mice fed CD or HFD. n = 5–6 mice per group; $^{*}P < 0.05$; $^{***}P < 0.001$. (**E**) H&E–stained eWAT from mice fed CD or HFD. (**F**) Cell area of eWAT. n = 5–9 mice per group, 100 cells measured per mouse; $^{**}P < 0.01$.

We considered the possibility that the obese phenotype in TgβARKct mice was due to increased food consumption when placed on the HFD. However, daily food intake did not differ between TgβARKct and NLC mice on either diet when measured across multiple consecutive 24-hour periods (Figure 2, E and F). This finding indicated that the different rates of weight gain in our mice is not related to satiety.

Leptin, an adipokine that regulates energy balance by inhibiting hunger, is also referred to as the obesity hormone, because leptin levels positively correlate with the extent of obesity, due to the development of leptin resistance. In agreement with the enhanced obesity observed in TgβARKct mice fed an HFD, we

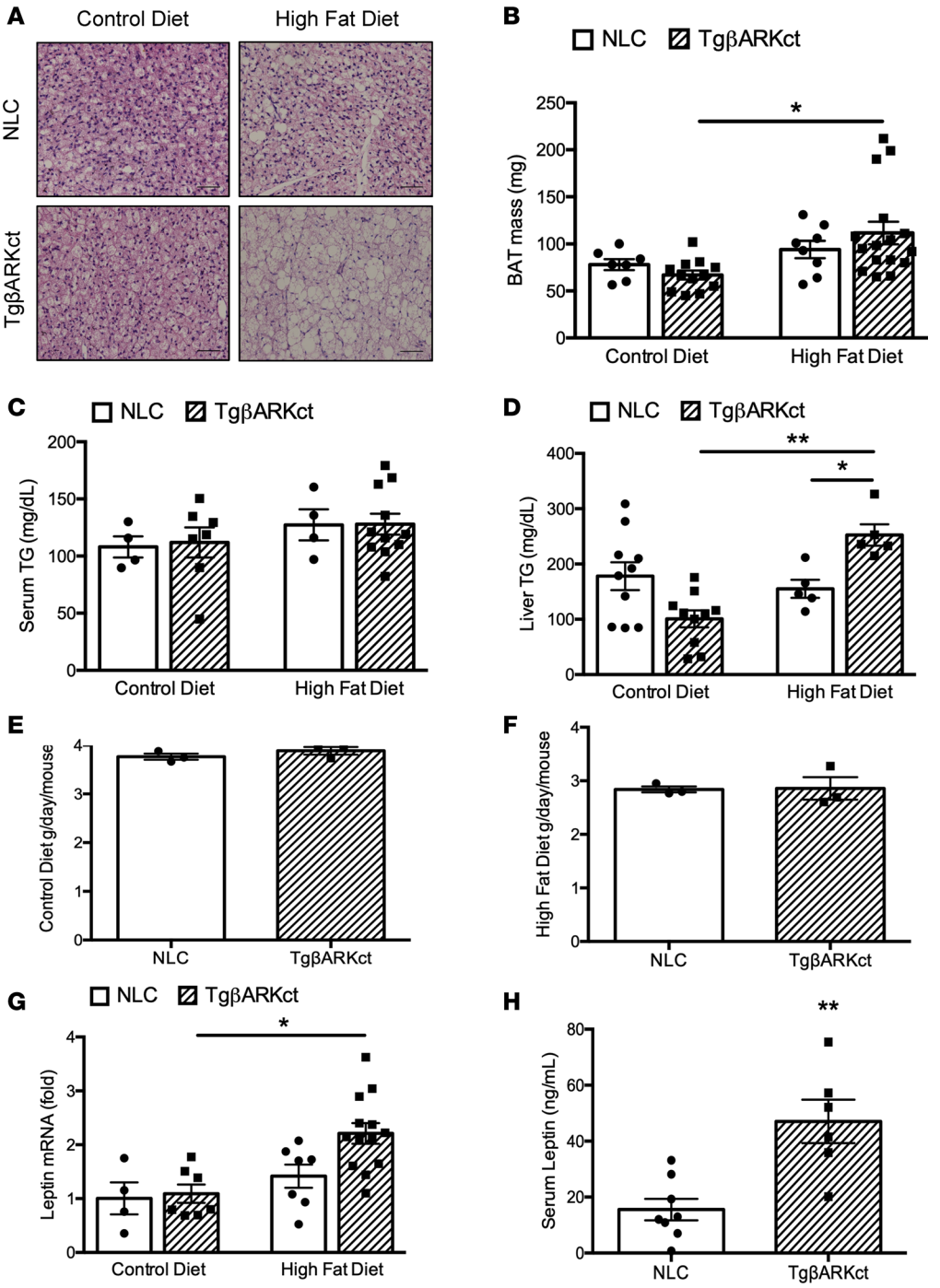

Figure 2. BAT weight is increased in TgβARKct animals following HFD. (**A**) H&E stain of BAT from TgβARKct and NLC mice fed CD or HFD. (**B**) Mass of BAT isolated from TgβARKct and NLC mice fed CD or HFD for 6 weeks. *n* = 4–7 mice per group; **P* < 0.05. (**C**) Serum triglyceride levels in TgβARKct and NLC mice fed CD or HFD for 6 weeks. *n* = 4–11 mice per group. (**D**) Liver triglyceride levels in TgβARKct and NLC mice fed CD or HFD for 6 weeks. *n* = 5–10 mice per group; **P* < 0.05; ***P* < 0.01. (**E** and **F**) average daily food intake of TgβARKct and NLC mice fed CD or HFD. Food intake was monitored daily in cages housing 4 mice of the same genotype. Five independent measurements at 24-hour intervals were recorded per cage and averaged. *n* = 3–4 cages per genotype. (**G**) Leptin mRNA expression in eWAT from TgβARKct or NLC mice fed CD or HFD for 6 weeks. *n* = 4–13 mice per group; **P* < 0.05. H, serum leptin from TgβARKct or NLC mice fed HFD. *n* = 6–8 mice per group; ***P* < 0.01.

saw increased leptin mRNA expression in the eWAT of TgβARKct mice relative to controls (Figure 2G). In addition, leptin levels measured in the serum were higher in HFD-fed TgβARKct mice compared with NLCs (Figure 2H).

TgGRK2 mice are resistant to HFD-induced obesity. Because cardiac-specific GRK2 inhibition in TgβARKct mice enhances susceptibility to HFD-induced obesity, we next asked whether cardiac overexpression of GRK2 would offer resistance to this effect. TgGRK2 mice display an approximately 3-fold overexpression of GRK2 exclusively in cardiomyocytes, which is similar to the upregulation seen in the failing human heart (Supplemental Figure 1B and ref. 12). Notably, TgGRK2 mice fed an HFD only increased their body weight by 27% within 6 weeks, whereas their corresponding NLC mice gained 49% body weight during the same time period (Figure 3, A and B, and Supplemental Figure 2B). Again, this metabolic phenotype only becomes apparent with HFD; we observed no difference in weight gain between TgGRK2 and NLC mice during 6 weeks on the CD (Figure 3, A and B).

In contrast to TgβARKct animals, visceral white adipose fat pads were significantly smaller in HFD-fed TgGRK2 mice compared with NLC mice (Figure 3, C and D). Again, as with the TgβARKct mice, we found the differences in adipose mass between TgGRK2 and NLC mice to be HFD dependent, with no baseline difference between mice fed CD (Figure 3, C and D). In support of the adipose weight data, histological analysis of eWAT revealed significant resistance to adipocyte hypertrophy in HFD-fed TgGRK2 mice relative to the NLC group (Figure 3, E and F). Similarly, we observed a significant decrease in subscapular BAT mass of TgGRK2 mice fed HFD relative to NLC mice (Figure 4B). BAT histology of HFD-fed TgGRK2 mice demonstrated reduced adipocyte hypertrophy and lipid storage compared with NLC mice (Figure 4A). Resistance to weight gain in TgGRK2 mice was not caused by differences in systemic respiration or physical activity, as calculated by measurements done within metabolic cages (Supplemental Figure 4, A–F).

Although not statistically significant, levels of serum triglycerides trended lower in TgGRK2 mice compared with NLCs on both diets, particularly those on the HFD (Figure 4C). This indication of lower body lipid content would be consistent with the obesity-resistant phenotype in the TgGRK2 mice. Mirroring serum triglyceride levels, we see a similar (nonsignificant) decrease in liver triglycerides of TgGRK2 mice in both diets, which is again, more pronounced in the HFD-fed group (Figure 4D).

As with the TgβARKct mice, we considered the possibility that the obesity-resistance phenotype in TgGRK2 mice was a result of altered food consumption when placed on an HFD. In agreement with data from the TgβARKct mice, however, daily food intake did not differ between TgGRK2 and NLC mice on either diet when measured across multiple consecutive 24-hour periods (Figure 4, E and F). This finding reinforced the conclusion that weight gain differences due to altered cardiac GRK2 activity are not caused by changes in satiety. Leptin expression was increased in the eWAT of HFD-fed NLC mice, however, in agreement with the obesity-resistant phenotype, we found no significant increase in leptin mRNA expression in the eWAT of HFD-fed TgGRK2 mice relative to animals on the CD (Figure 4G).

WAT from TgβARKct mice shows increased expression of genes related to adipose differentiation and function. A particularly striking aspect of the metabolic phenotype in our transgenic mice is the rapid expansion of adipose tissue depots in the TgβARKct mice fed an HFD. Conversely, adipose tissue mass is significantly restricted in HFD-fed TgGRK2 mice. In light of these observations, we considered whether regulation of adipose differentiation and function is altered in our transgenic mice. To explore this possibility, we analyzed the expression of key regulators of these processes in WAT harvested from TgβARKct, TgGRK2, and NLC mice fed either CD or HFD for 6 weeks. Interestingly, expression of KLF5, an early regulator of adipocyte differentiation, was significantly increased in TgβARKct mice fed CD, whereas no change was observed in TgGRK2 mice on CD (Figure 5A). Furthermore, expression of sterol regulatory element binding protein-1c (SREBP-1c), another key regulator of adipogenesis, was significantly increased in TgβARKct mice fed HFD, while again, no such change was observed in TgGRK2 mice (Figure 5B). Finally, we found significantly higher glucose transporter type 4 (GLUT4) expression in the adipose tissue of TgβARKct mice on HFD, compared with NLC mice, whereas, once again, we found no such expression differences in the TgGRK2 mice (Figure 5C). Taken together, these results suggest that adipocyte differentiation may be enhanced in the WAT tissue of TgβARKct mice. Furthermore, having greater GLUT4 expression, TgβARKct adipocytes may be better adapted for energy uptake and storage.

Metabolomic analysis of heart tissue and serum in TgGRK2 and TgβARKct mice on CD and HFD. To better characterize the metabolic phenotype of our transgenic mice and to possibly assist in identifying a

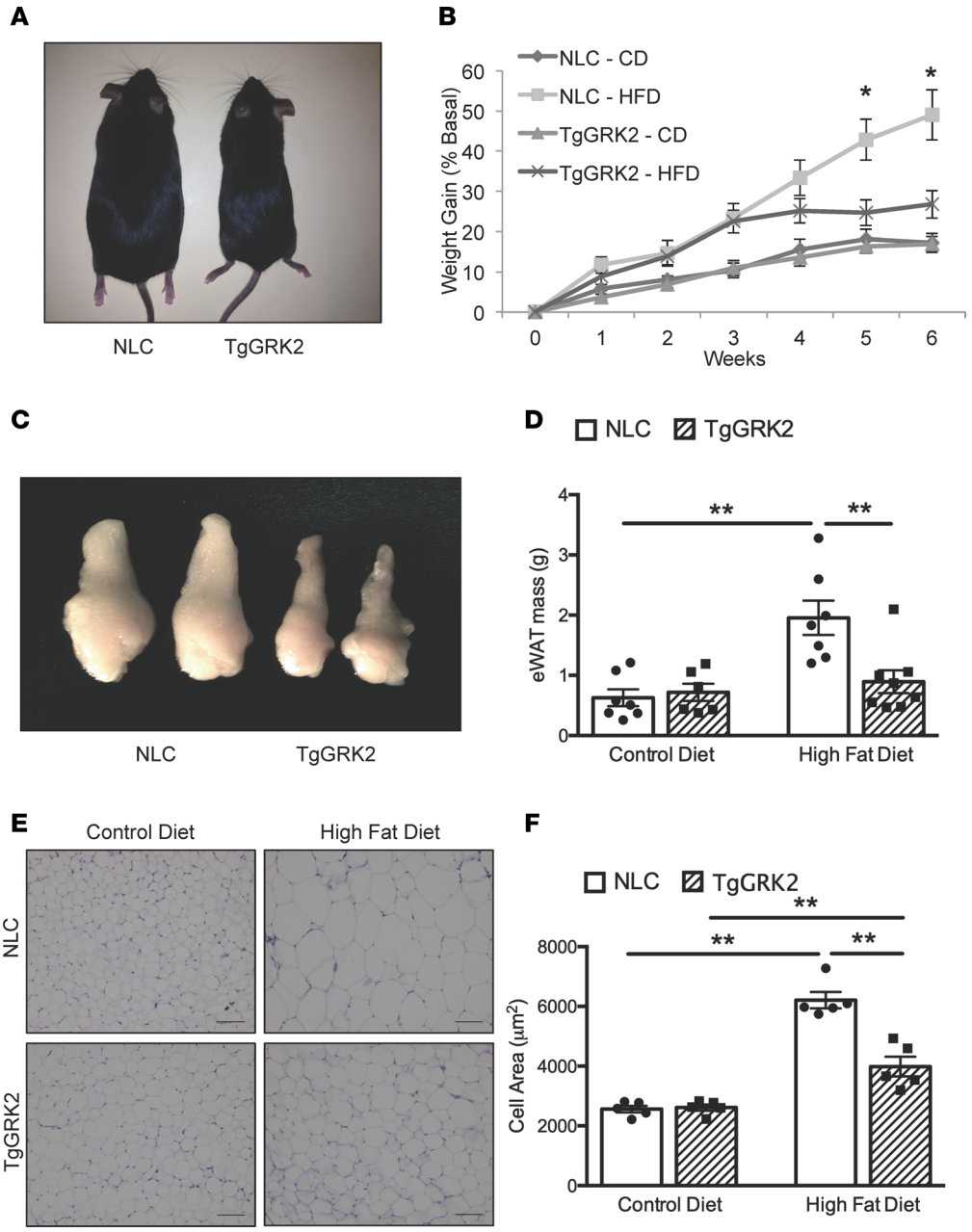

Figure 3. TgGRK2 mice display resistance to diet-induced obesity. (**A**) TgGRK2 and NLC mice following 6 weeks of HFD compared to the same mice fed CD. (**B**) Percentage weight gain of TgGRK2 and NLC mice fed CD or HFD for 6 weeks. n = 7–11 mice per group; $^{*}P < 0.05$. (**C**) Representative gross images of eWAT from TgGRK2 and NLC mice after HFD. (**D**) Mass of eWAT isolated from TgGRK2 and NLC mice fed CD or HFD. n = 4–5 mice per group; $^{*}P < 0.05$; $^{**}P < 0.01$. (**E**) H&E–stained eWAT from mice fed CD or HFD. (**F**) Cell area of eWAT. n = 5 mice per group, 100 cells measured per mouse; $^{**}P < 0.01$.

cardiac-generated signaling molecule, we analyzed the metabolome of serum and heart tissue in our transgenic mice and respective NLCs in response to control or HFD feeding. The resulting dataset comprises a total of 579 compounds of known identity in the heart and 556 in the serum. ANOVA contrasts identified numerous biochemicals that differed significantly between experimental groups, as shown in Tables 1–4. Furthermore, analysis by 2-way ANOVA identified biochemicals exhibiting significant main effects and interactions for experimental parameters of genotype and diet (Tables 1–4).

Differential regulation of BCAA metabolism in TgGRK2 and TgβARKct mice fed an HFD. When the TgβARKct mice were compared with their NLC mice under the HFD condition, they exhibited significant increases in the myocardium of several metabolites belonging to the BCAA pathway, including α-hydroxyisovalerate (HIVA) and 2-hydroxy-3-methylvalerate (HMVA, Table 5). Interestingly, several of these increases were also

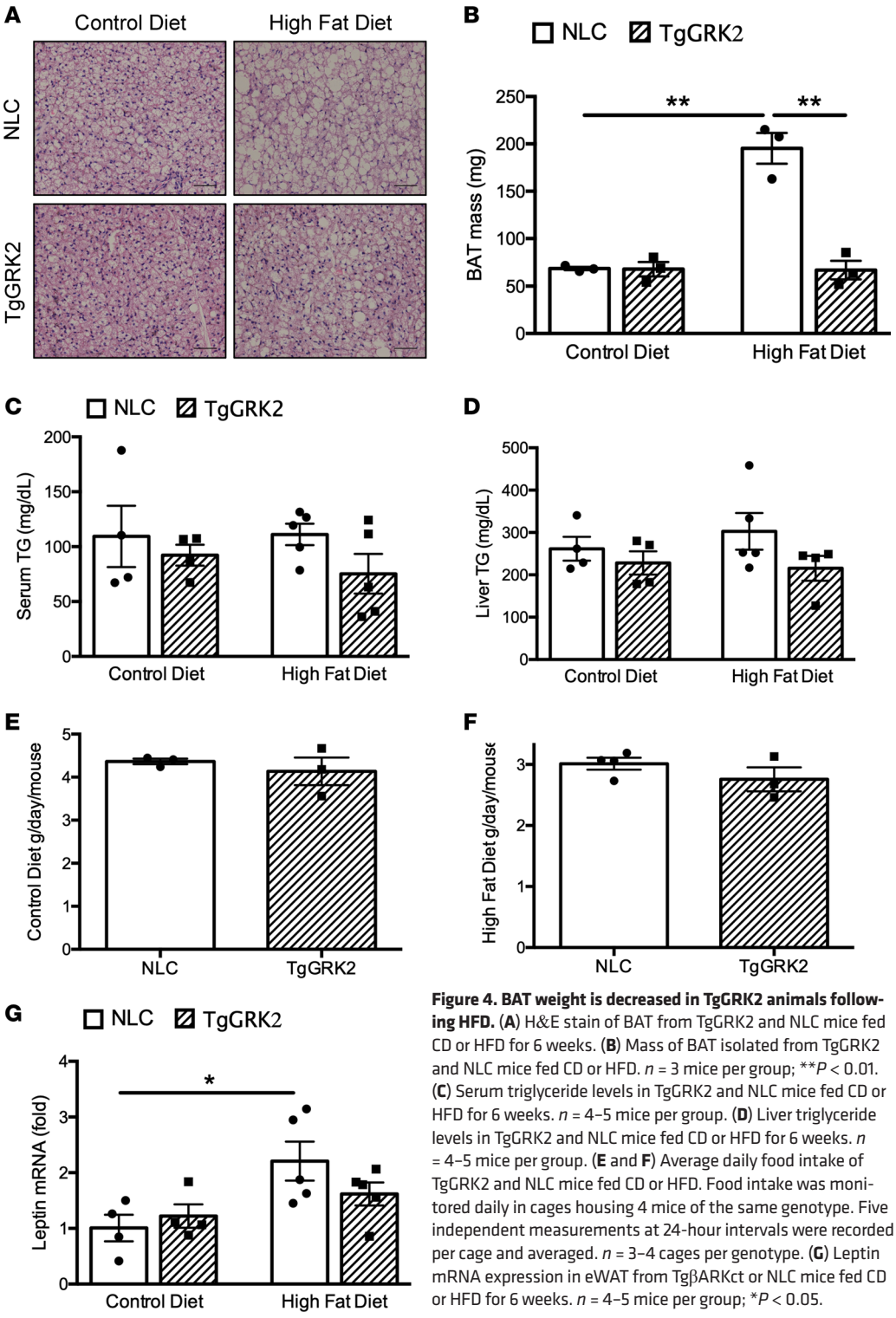

Figure 4. BAT weight is decreased in TgGRK2 animals following HFD. (**A**) H&E stain of BAT from TgGRK2 and NLC mice fed CD or HFD for 6 weeks. (**B**) Mass of BAT isolated from TgGRK2 and NLC mice fed CD or HFD. $n = 3$ mice per group; $^{**}P < 0.01$. (**C**) Serum triglyceride levels in TgGRK2 and NLC mice fed CD or HFD for 6 weeks. $n = 4–5$ mice per group. (**D**) Liver triglyceride levels in TgGRK2 and NLC mice fed CD or HFD for 6 weeks. $n = 4–5$ mice per group. (**E** and **F**) Average daily food intake of TgGRK2 and NLC mice fed CD or HFD. Food intake was monitored daily in cages housing 4 mice of the same genotype. Five independent measurements at 24-hour intervals were recorded per cage and averaged. $n = 3–4$ cages per genotype. (**G**) Leptin mRNA expression in eWAT from TgβARKct or NLC mice fed CD or HFD for 6 weeks. $n = 4–5$ mice per group; $^{*}P < 0.05$.

echoed in the serum of the TgβARKct animals (Table 6). Conversely, the HFD TgGRK2 mice exhibited a decrease in numerous members of the BCAA pathway in both the heart and the serum (Tables 5 and 6). Changes in serum BCAA metabolites were separately validated using hydrophilic interaction ultra-performance liquid chromatography tandem mass spectrometry (ILIC/UPLC-MS/MS) with negative ion mode electrospray ionization (ESI) in TgGRK2 and TgβARKct samples (Supplemental Figure 5, A and B). The opposite outcome for BCAA metabolism in TgGRK2 versus TgβARKct mice suggests that GRK2 activity levels may directly influence the regulation of this pathway. Furthermore, it is therefore possible that changes

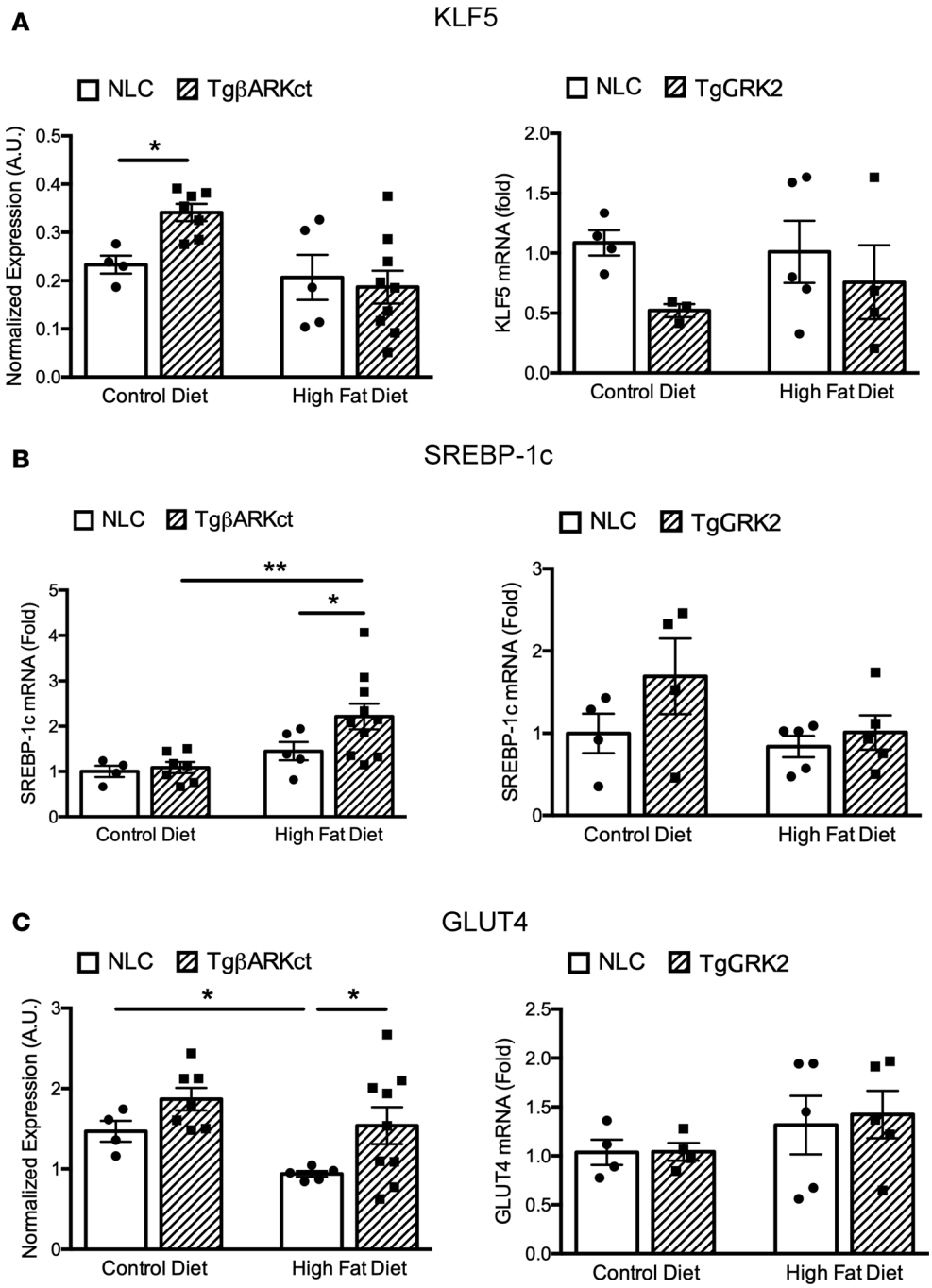

Figure 5. Expression of genes related to adipose function and differentiation in WAT of TgGRK2 and TgβARKct mice. Expression analysis of KLF5 (**A**), SREBP-1c (**B**), and GLUT4 (**C**), in the WAT of TgβARKct mice (left panels) and TgGRK2 mice (right panels) and respective NLC mice fed CD or HFD for 6 weeks. n = 4–9 mice per group; $^{*}P < 0.05$; $^{**}P < 0.01$.

seen in the serum originate in the heart where GRK2 activity is altered. Interestingly, circulating BCAA concentrations have previously been linked with obesity and development of insulin resistance (24).

Differential regulation of endocannabinoid pathway metabolism in TgGRK2 and TgβARKct mice fed an HFD. When the TgβARKct mice were compared to NLCs fed an HFD, they exhibited significant increases in several cardiac metabolites belonging to the endocannabinoid pathway, including *N*-oleoyl taurine and *N*-palmitoyl taurine (Table 7). Furthermore, to a lesser degree, this pattern of increase for members of this pathway was also evident in the serum of the TgβARKct animals (Table 8). Conversely, the TgGRK2 mice fed an HFD exhibited a significant decrease in *N*-oleoyl taurine and *N*-palmitoyl taurine in the heart, while levels in the serum were mostly unchanged, aside from a decrease in oleoylethanolamide (Tables 7 And 8). The

Table 1. Statistical summary of heart tissue metabolite profile differences between TgβARKct and NLC mice fed CD or HFD

	Statistical comparison (heart)			
ANOVA contrasts	**NLC βARKct HFD / NLC βARKct CD**	**Tg-βARKct HFD / Tg-βARKct CD**	**Tg-βARKct CD / NLC βARKct CD**	**Tg-βARKct HFD / NLC βARKct HFD**
Total biochemicals $P \leq 0.05$	142	100	93	106
Biochemicals (↑|↓)	↑ 34 | 108 ↓	↑ 36 | 64 ↓	↑ 50 | 43 ↓	↑ 72 | 34 ↓
Total biochemicals $0.05 < P < 0.10$	53	43	55	50
Biochemicals (↑|↓)	↑ 16 | 37 ↓	↑ 17 | 26 ↓	↑ 28 | 27 ↓	↑ 37 | 13 ↓
Two-way ANOVA	**Genotype Main Effect (βARKct)**	**Diet Main Effect (βARKct)**	**Genotype: Diet Interaction (βARKct)**	
Total biochemicals $P \leq 0.05$	118	143	68	
Total biochemicals $0.05 < P < 0.10$	39	57	54	

opposite pattern of results of endocannabinoid metabolites in TgGRK2 versus TgβARKct mice suggests that GRK2 activity levels may directly influence the regulation of this pathway. This could be of significant interest to our study, as endocannabinoids have well-characterized metabolic signaling roles including regulation of adipogenesis and lipid metabolism (25).

Circulating BCAA metabolite altered by cardiac GRK2 signaling during an HFD modulate adipogenesis. Based on the results presented here, we hypothesized that one or more of the circulating metabolites differentially regulated by GRK2 signaling in the heart was acting as a cardiac-generated signaling molecule. The α-hydroxy BCAA metabolites (HIVA, α-hydroxyisocaproate [HICA], and HMVA) were identified as potential targets because (a) serum levels closely corresponded with metabolic phenotype (higher in TgβARKct animals and lower in TgGRK2 animals) and (b) serum and myocardial levels were closely correlated in each line (Table 5). To test the hypothesis that these are cardiac-derived metabolites signaling to adipose tissue, we developed an in vitro assay using 3T3-L1 pre-adipocyte cells, which can be stimulated to differentiate into adipocytes (via addition of insulin, isobutylmethylxanthine, and dexamethasone) and are commonly used as a model to study adipogenesis. We differentiated 3T3-L1 adipocytes in differentiation media containing the α-hydroxy BCAA metabolites for 8 days and determined the extent of differentiation using BODIPY 493/503 staining of neutral lipids in mature adipocytes. Although 2 of the metabolites (HIVA and HICA) had no effect on 3T3-L1 differentiation, cells differentiated in

Table 2. Statistical summary of serum metabolite profile differences between TgβARKct and NLC mice fed CD or HFD

	Statistical comparison (serum)			
ANOVA contrasts	**NLC βARKct HFD / NLC βARKct CD**	**Tg-βARKct HFD / Tg-βARKct CD**	**Tg-βARKct CD / NLC βARKct CD**	**Tg-βARKct HFD / NLC βARKct HFD**
Total biochemicals $P \leq 0.05$	74	117	53	58
Biochemicals, (↑|↓)	↑ 25 | 49 ↓	↑ 47 | 70 ↓	↑ 38 | 15 ↓	↑ 43 | 15 ↓
Total biochemicals $0.05 < P < 0.10$	45	63	67	44
Biochemicals, (↑|↓)	↑ 12 | 33 ↓	↑ 22 | 41 ↓	↑ 44 | 23 ↓	↑ 32 | 12 ↓
Two-way ANOVA	**Genotype Main Effect (βARKct)**	**Diet Main Effect (βARKct)**	**Genotype: Diet Interaction (βARKct)**	
Total biochemicals $P \leq 0.05$	61	126	51	
Total biochemicals $0.05 < P < 0.10$	48	46	49	

Table 3. Statistical summary of heart tissue metabolite profile differences between TgGRK2 and NLC mice fed CD or HFD

	Statistical comparison (heart)			
ANOVA contrasts	**NLC GRK2 HFD / NLC GRK2 CD**	**Tg-GRK2 HFD / Tg-GRK2 CD**	**Tg-GRK2 CD / NLC GRK2 CD**	**Tg-GRK2 HFD / NLC GRK2 HFD**
Total biochemicals $P \leq 0.05$	157	199	57	55
Biochemicals (↑↓)	↑ 90 | 67 ↓	↑ 93 | 106 ↓	↑ 35 | 22 ↓	↑ 21 | 34 ↓
Total biochemicals $0.05 < P < 0.10$	43	50	38	37
Biochemicals, (↑↓)	↑ 26 | 17 ↓	↑ 28 | 22 ↓	↑ 10 | 28 ↓	↑ 9 | 28 ↓
Two-way ANOVA	**Genotype Main Effect (GRK2)**	**Diet Main Effect (GRK2)**	**Genotype: Diet Interaction (GRK2)**	
Total biochemicals $P \leq 0.05$	56	228	56	
Total biochemicals $0.05 < P < 0.10$	45	43	34	

the presence of HMVA showed significantly increased lipid accumulation (Figure 6, A and B). HMVA showed a dose-dependent enhancement of lipid accumulation in differentiated 3T3-L1 cells (Figure 6C), suggesting HMVA is a novel regulator of adipocyte differentiation. These results suggest that changes in BCAA metabolism in the heart due to GRK2 signaling could alter circulating BCAA metabolite levels to influence weight gain on an HFD mouse.

Discussion

The canonical role of GRK2 in GPCR desensitization is well characterized. This is especially true in the setting of the myocardium, where more than 2 decades of research have demonstrated the importance of GRK2 in normal heart function, in addition to the maladaptive role of GRK2 upregulation following injury and in HF. In recent years, several groups have identified novel, noncanonical signaling roles for GRK2 involving targets other than GPCRs. Furthermore, many of these novel targets and roles for GRK2 implicate GRK2 as a metabolic regulator (19, 20). GRK2 activity appears to have an effect on metabolic rate in several tissues, including adipose, because global reduction in GRK2 levels seems to offer modest resistance to HFD-induced weight gain and insulin resistance (22, 23).

Moving forward, the original goal of our study was to further examine the role of GRK2 activity in the development of cardiac insulin resistance and diabetic cardiomyopathy following HFD. While pursuing this, we made the unexpected discovery that cardiac GRK2 activity is linked to global energy homeostasis. TgβARKct mice were more susceptible to HFD-induced obesity, whereas TgGRK2 mice showed resistance to weight gain on an HFD relative to control animals. Interestingly, these metabolic phenotypes only

Table 4. Statistical summary of serum metabolite profile differences between TgGRK2 and NLC mice fed CD or HFD

	Statistical comparison (serum)			
ANOVA contrasts	**NLC GRK2 HFD / NLC GRK2 CD**	**Tg-GRK2HFD / Tg-GRK2 CD**	**Tg-GRK2CD / NLC GRK2 CD**	**Tg-GRK2HFD / NLC GRK2 HFD**
Total biochemicals $P \leq 0.05$	121	203	75	58
Biochemicals (↑↓)	↑ 55 | 66 ↓	↑ 80 | 123 ↓	↑ 45 | 30 ↓	↑ 14 | 44 ↓
Total biochemicals $0.05 < P < 0.10$	46	48	51	38
Biochemicals (↑↓)	↑ 24 | 22 ↓	↑ 22 | 26 ↓	↑ 24 | 27 ↓	↑ 15 | 23 ↓
Two-way ANOVA	**Genotype Main Effect (GRK2)**	**Diet Main Effect (GRK2)**	**Genotype: Diet Interaction (GRK2)**	
Total biochemicals $P \leq 0.05$	35	192	79	
Total biochemicals $0.05 < P < 0.10$	35	52	38	

Table 5. Heatmap of statistically significant differences in BCAA metabolism intermediates in TgβARKct, TgGRK2, and NLC hearts

Subpathway	Biochemical name	Tg-βARKct HFD / NLC βARKct HFD	Tg-GRK2 HFD / NLC GRK2 HFD
BCAA metabolism	*N*-acetylleucine	1.26	0.6[B]
	4-methyl-2-oxopentanoate	1.03	0.72
	β-hydroxyisovalerate	1.22	0.68[B]
	HIVA	1.58[A]	0.57[B]
	isoleucine	1.17[A]	1
	N-acetylisoleucine	1.71[C]	0.54
	tiglycarnitine	1.49	0.69[D]
	HMVA	1.9[A]	0.6[D]
	3-hydroxy-2-ethylpropionate	0.98	0.96
	ethylmalonate	1.14	0.88
	valine	1.16[A]	0.97
	HICA	2.84[A]	0.88

[A]Indicates that the mean values are significantly higher for that comparison. $P \le 0.05$. [B]Indicates that the mean values are significantly lower for that comparison. $P \le 0.05$. [C]Indicates that the mean values trend higher for that comparison. $0.05 < P < 0.10$. [D]Indicates that the mean values trend lower for that comparison. $0.05 < P < 0.10$.

became apparent when mice were fed an HFD; no difference in weight gain was observed in either transgenic mouse when fed a CD. Importantly, food intake and physical activity did not differ between GRK2 or βARKct transgenic mice and their NLC controls, suggesting that the phenotypes observed are not related to changes in satiety or relative activity levels.

It is notable that these metabolic phenotypes were entirely unexpected, not least because the TgβARKct and TgGRK2 mice express their respective transgenes in a cardiac-specific manner via the α-myosin heavy-chain (α-MHC) promoter. Interestingly, although we find cardiac-specific inhibition of GRK2 results in enhanced obesity when placed on HFD, others have shown that global downregulation of GRK2 in all tissues of the body results in the opposite phenotype, with these mice displaying mild resistance to HFD-induced weight gain (22, 23, 26). In these studies, reduction in GRK2 expression in WAT and BAT seems to have a profound effect on adipose tissue homeostasis. WAT in GRK2 hemizygous mice exhibits decreased expression of several genes involved in lipogenesis, while expression of lipolysis-related genes are increased. Furthermore, BAT from GRK2 hemizygous mice shows a gene expression profile that would favor enhanced thermogenesis in these animals. GRK2 hemizygous mice display increased thermogenic

Table 6. Heatmap of statistically significant differences in BCAA metabolism intermediates in TgβARKct, TgGRK2, and NLC serum

Subpathway	Biochemical name	Tg-βARKct HFD / NLC βARKct HFD	Tg-GRK2 HFD / NLC GRK2 HFD
BCAA metabolism	*N*-acetylleucine	1.73[C]	1.07
	4-methyl-2-oxopentanoate	1.69[C]	0.91
	isovalerate	2.39[A]	0.5
	3-methylglutaconate	1.21	0.66[B]
	HIVA	1.62[A]	0.59[B]
	N-acetylisoleucine	1.4[C]	0.97
	HMVA	1.92[A]	0.6[D]
	3-hydroxy-2-ethylpropionate	1.34	0.58[B]
	ethylmalonate	1.19	0.77[D]
	HICA	1.73[A]	0.67[B]

[A]Indicates that the mean values are significantly higher for that comparison. $P \le 0.05$. [B]Indicates that the mean values are significantly lower for that comparison. $P \le 0.05$. [C]Indicates that the mean values trend higher for that comparison. Values for each sample are normalized by the volume of serum extracted. $0.05 < P < 0.10$. [D]Indicates that the mean values trend lower for that comparison. Values for each sample are normalized by the volume of serum extracted. $0.05 < P < 0.10$.

Table 7. Heatmap of statistically significant differences in endocannabinoid pathway intermediates in TgβARKct, TgGRK2, and NLC hearts

Subpathway	Biochemical name	Tg-βARKct HFD / NLC βARKct HFD	Tg-GRK2 HFD / NLC GRK2 HFD
Endocannabinoid	oleoyl ethanolomide	1.73[A]	0.82
	palmitoyl ethanolamide	1.65[A]	0.94
	stearoyl ethanolomide	1.27	0.96
	arachidonoyl ethanolamide	1.15	0.9
	N-oleoyltaurine	2.26[A]	0.66[B]
	N-stearoyltaurine	2.58[A]	0.84
	N-palmitoyltaurine	2.25[A]	0.61[B]
	linoleoyl ethanolamide	1.42	0.94

[A]Indicates that the mean values are significantly higher for that comparison. $P \leq 0.05$. [B]Indicates that the mean values are significantly lower for that comparison. $P \leq 0.05$.

capacity, by way of increased core body temperature and respiratory exchange ratio, which in the absence of changes in physical activity, suggests a more oxidative phenotype in the BAT and WAT (26). It is therefore possible that the metabolic phenotype we observe, originating from reduction in GRK2 activity in the heart, is masked in the global GRK2 hemizygous mice, by direct GRK2-dependent effects in other tissue types, primarily in the adipose.

We also considered that the weight-gain phenotype might be a direct result of differences in cardiac energy homeostasis in the TgGRK2 and TgβARKct mice. The heart consumes more oxygen per gram than any tissue in the body in order to maintain production of the massive quantities of ATP required for sustained contractile function (27). It is therefore possible that a perturbation in energy production/usage by the heart could result in an energy imbalance affecting the whole animal. However, recent data from our lab have shown that GRK2 inhibition in NRVMs increased ATP-linked respiration and the basal respiratory rate was measured using a Seahorse flux analyzer (Agilent) (20). This finding would suggest that energy expenditure in TgβARKct hearts might even be higher than in NLC hearts, which would be the opposite of what we would expect, if the obese phenotypes of these mice were a direct consequence of altered cardiac metabolism. Instead, these results imply the metabolic phenotypes arising from modulation of cardiac GRK2 activity involve peripheral tissues beyond the myocardium.

Interest in the regulation of global metabolism by interorgan communication has intensified in recent years; the endocrine signaling function of adipose tissue is perhaps the best-characterized example (28, 29). Various adipokines, such as leptin, resistin, and adiponectin are secreted from adipose tissue depots in the

Table 8. Heatmap of statistically significant differences in endocannabinoid pathway intermediates in TgβARKct, TgGRK2, and NLC serum

Subpathway	Biochemical name	Tg-βARKct HFD / NLC βARKct HFD	Tg-GRK2 HFD / NLC GRK2 HFD
Endocannabinoid	oleoyl ethanolomide	1.58	0.8[B]
	palmitoyl ethanolamide	1.37	1.01
	stearoyl ethanolomide	1.33[C]	1
	arachidonoyl ethanolamide	1.51[C]	0.86
	N-oleoyltaurine	1.39	0.93
	N-stearoyltaurine	1.11	0.93
	N-palmitoyltaurine	2.61	0.92
	linoleoyl ethanolamide	1.62[A]	0.88

[A]Indicates that the mean values are significantly higher for that comparison. $P \leq 0.05$. [B]Indicates that the mean values are significantly lower for that comparison. $P \leq 0.05$. [C]Indicates that the mean values trend higher for that comparison. Values for each sample are normalized by the volume of serum extracted. $0.05 < P < 0.10$.

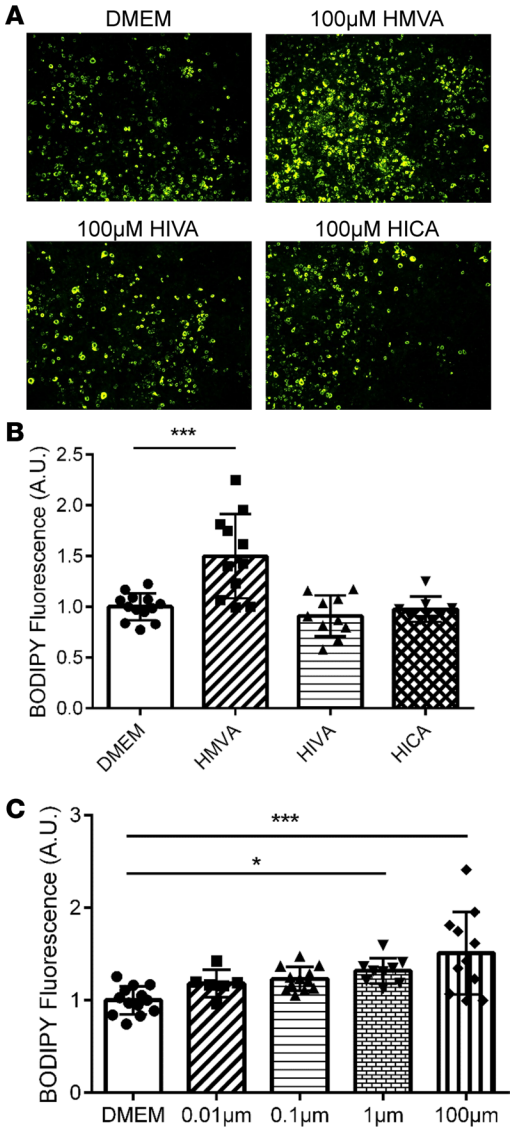

Figure 6. 3T3-L1 adipocyte differentiation is enhanced in the presence of the BCAA metabolite HMVA. (**A**) Representative BODIPY 493/503–stained 3T3-L1 cells differentiated in the presence of 2-hydroxy BCAA metabolites. 3T3-L1 cells were subjected to adipocyte differentiation for 8 days in differentiation media containing α-hydroxy BCAA metabolites. (**B**) Summary data for BODIPY staining of differentiated 3T3-L1 cells. n = 8–11 per condition; $^{***}P < 0.001$. (**C**) The α-hydroxy BCAA metabolite HMVA increases 3T3-L1 in a dose-dependent manner. $^{*}P < 0.05$; $^{***}P < 0.001$.

body and communicate with distant tissues, eliciting metabolic changes within those tissues, and thereby modifying global metabolism to adapt to environmental inputs such as nutritional status (30).

Other tissues have been shown to communicate in a similar manner to adipose. For instance, irisin secretion from skeletal muscle can induce browning of WAT, promoting energy expenditure and resistance to obesity (4). Similarly, natriuretic peptides secreted by the heart can stimulate thermogenesis and energy expenditure in adipose tissue (31). Gene expression changes in the adipose tissue of our cardiac-specific transgenic mice suggest that GRK2 may regulate a communicative link between these 2 tissues. In recent years, studies have identified a third class of adipose tissue, commonly referred to as beige fat (32). Beige fat exists within the WAT and is believed to occur as a consequence of "browning" of white adipocytes, referring to the reprogramming of white adipocytes to adopt the characteristics of brown adipocytes, such as increased lipolysis, uncoupled respiration, and mitochondrial content. One of the consequences of having more beige fat present within WAT is increased energy expenditure and therefore a leaner body composition. WAT from HFD-fed TgβARKct mice seemed to lack any such characteristics, with increased adipocyte differentiation, expression of fat storage genes, and enhanced lipid uptake and adipocyte hypertrophy instead.

To aid in our search for a GRK2-regulated, cardiac-secreted molecule and to better characterize the phenotypes of our transgenic mice, we conducted a metabolomic analysis of heart tissue and serum. This approach identified numerous differences between TgGRK2 and TgβARKct mice and their respective littermate controls on both CD and HFDs. Two-way ANOVA analysis found both genotype and diet-related effects on the

metabolic profiles. Levels of BCAA metabolites showed an inverse relationship between HFD-fed TgβARKct and TgGRK2 mice. Heart and serum levels were increased in TgβARKct animals and decreased in TgGRK2. The role of BCAA in metabolic signaling and insulin resistance is somewhat controversial. On the one hand, many reports have suggested that increased levels of BCAA have beneficial effects on various aspects of obesity and metabolic syndrome including satiety and glycemia (33–35). On the other hand, several studies link elevated BCAA levels with obesity and extent of insulin resistance (36–38). Additional evidence demonstrates that BCAA metabolism plays a critical role in regulating adipocyte differentiation and lipid synthesis. Adipocyte differentiation increases the expression of enzymes responsible for BCAA catabolism, including branched-chain aminotransferase 2 and branched-chain α-keto acid dehydrogenase complex (39, 40). After adipocyte differentiation, BCAA catabolism significantly increases the lipogenic acetyl-CoA, and propionyl-CoA pools to increase lipid accumulation (39, 41, 42). Further, removing BCAAs from the media inhibits adipogenesis (39), demonstrating a critical role for BCAA metabolism in regulating adipocyte differentiation and lipid handling.

Here, we show that circulating BCAA metabolites altered by GRK2 signaling within the myocardium can enhance adipocyte differentiation using an in vitro 3T3-L1 assay. This BCAA metabolite could serve as a novel signaling factor that communicates cardiac metabolic state to adipose tissue to match energy storage and utilization. A recent study identified the α-hydroxy BCAA metabolites as secondary messengers that modulate the osmotic stress response in yeast through modification of GPCR signaling (43), demonstrating a physiological role for these metabolites. Additionally, another BCAA metabolite released from skeletal muscle cells increases endothelial and skeletal muscle fatty acid uptake and can cause glucose intolerance (44), emphasizing the importance of BCAA metabolism in regulating metabolic health. Interestingly, myocardial BCAA metabolism is also altered in heart failure, a condition known to increase GRK2 signaling within the myocardium (45, 46). It is possible that altered BCAA metabolism during HF due to enhanced GRK2 signaling could play an important role in modulating global health and insulin signaling.

In addition to BCAA metabolites, endocannabinoid levels showed a similar inverse relationship between HFD-fed TgβARKct and TgGRK2 mice. Cardiac levels of several endocannabinoid metabolites were increased in TgβARKct animals and decreased in TgGRK2. This pattern was mirrored to a lesser extent in the serum of these mice. This result could be of great importance because endocannabinoids are known to have significant effects on energy balance. Endocannabinoids have a well-characterized signaling role in the brain, regulating hypothalamic circuits to modulate satiety and food intake (47). However, recent research has revealed the presence of endocannabinoid receptors in peripheral tissues, including adipose. Activation of the peripheral endocannabinoid system has been implicated in the development of obesity (48). Stimulation of adipose cannabinoid receptor type 1 (CB1) endocannabinoid receptors has been shown to enhance adipogenesis, lipogenesis, and glucose uptake (25). Activation of the CB1 receptor has similarly been shown to increase fatty acid synthesis in the liver via activation of the transcription factor SREBP-1c, a critical regulator of lipid synthesis pathways, which we also find to be elevated in TgβARKct WAT mice (49). Furthermore, pharmacological inhibition of the CB1 receptor with rimonabant reduces food intake and weight loss via central and peripheral mechanisms (50). Given these effects of endocannabinoid signaling on global metabolism, and in particular on adipose tissue function, GRK2-mediated regulation of endocannabinoid metabolism in the heart clearly warrants further study. Endocannabinoids are formed in the cell membrane; phospholipids are the precursor and can follow one of many synthesis pathways en route to becoming an endocannabinoid (51). Tissue levels of endocannabinoids are also managed by degradation, with fatty acid amidohydrolase and monoglyceride lipase mostly responsible, although some other enzymes may contribute (52). Future studies should investigate the potential for regulation of endocannabinoid synthesis and degradation by GRK2. Interestingly, phospholipase C (PLC) catalyzes the first step in one of the potential synthesis pathways. PLC is activated downstream of Gq-coupled GPCRs, such as the angiotensin II type 1 receptor, which is regulated by GRK2 phosphorylation in the heart. This should be investigated as a potential mechanism for the increased endocannabinoid metabolism in TgβARKct, however, potential regulation of other enzymes in this pathway by GRK2 should not be excluded.

In summary, in this study, we identified metabolic phenotypes that arise from modulating GRK2 activity selectively and exclusively in the heart. We show that TgβARKct mice are more susceptible to HFD-induced obesity than those on the CD. TgβARKct mice exhibit a marked increase in adiposity on HFD relative to control animals. Conversely, TgGRK2 mice show resistance to weight gain on an HFD and a decrease in adipose tissue mass relative to control animals. Furthermore, serum and myocardial samples from TgβARKct and TgGRK2 mice displayed a number of changes in metabolic pathways that could potentially alter adipose tissue metabolism in vivo, including alterations in BCAA

and endocannabinoid metabolism. These results suggest GRK2 is a critical regulator of cardiac metabolism during HFD and that changes in myocardial metabolism are communicated with adipose tissue to modulate weight gain.

Methods

Mice

Eight- to 12-week-old male TgβARKct and TgGRK2 mice were used for all experiments, in addition to NLC animals from each line (12). All mice were from the C57BL/6 strain, and all animal studies were conducted with the approval of the Animal Care and Use Committee at Temple University.

Diet-induced obesity

HFD-induced obesity was conducted via ad lib feeding of a 60% kcal from fat diet (Open Source Diets, D12492). Control groups were fed a 10% kcal from fat diet (Open Source Diets, D12450B). All animals were between 8–12 weeks of age prior to HFD. Food intake on both diets was monitored daily in cages housing 4 mice of the same genotype. Five independent measurements at 24-hour intervals were recorded per cage and averaged. Three to 4 cages per genotype were studied in this manner. All animals were fasted for approximately 16 hours prior to euthanization and tissue harvest.

Immunoblotting

After sodium dodecyl sulfate–polyacrylamide gel electrophoresis and transfer to nitrocellulose membranes, primary antibody incubations were performed overnight at 4°C. Fluorescent secondary antibodies were obtained from LI-COR Biosciences. Membranes were scanned with the Odyssey infrared imaging system (LI-COR). Both GRK2 and GAPDH primary antibodies used were sourced from Santa Cruz Biotechnology.

Histology

WAT and BAT were isolated and fixed in 4% paraformaldehyde (PFA) for 24 hours. Following fixation, samples were paraffin embedded and 7-μm sections were cut using a microtome. Sections were stained with H&E and images were taken using a Nikon DS-Ri1. For eWAT cell area measurements, 100 adipocytes were measured per mouse, across multiple fields using ImageJ software (NIH).

Adipocyte differentiation of 3T3-L1 cells

3T3-L1 cells (ATCC) were subcultured at subconfluent density in DMEM supplemented with 10% FBS. To initiate adipocyte differentiation, cells were plated in 12-well culture dishes and allowed to reach confluence. Forty-eight hours later, media was aspirated from the cells and replaced with DMEM media supplemented with differentiation factors (1.0 μM dexamethasone, 0.5 mM methylisobutylxanthine, 1.0 μg/ml insulin). Forty-eight hours later, and every subsequent 48 hours, for the duration of the experiment, media was changed to DMEM media supplemented with 1.0 μg/ml insulin. After 8 days, differentiated 3T3-L1 adipocytes were washed with PBS and fixed with 4% PFA for 30 minutes. Fixed cells were stained for 30 minutes using the fluorescent BODIPY 493/503 probe that stains neutral lipids. The BODIPY 493/503–positive area within each field was then determined automatically by ImageJ.

Metabolomic analysis of heart and serum

Metabolomic analysis was conducted by Metabolon, Inc. following the process outlined in the information to follow.

Sample preparation. Following isolation, heart and serum samples were inventoried and immediately stored at –80°C. Each sample received was accessioned into the Metabolon Laboratory Information Management System (LIMS) and was assigned by the LIMS a unique identifier that was associated with the original source identifier only. This identifier was used to track all sample handling, tasks, results, etc. The samples (and all derived aliquots) were tracked by the LIMS system. All portions of any sample were automatically assigned their own unique identifiers by the LIMS when a new task was created; the relationship of these samples was also tracked. All samples were maintained at –80°C until processed. Samples were prepared using the automated MicroLab STAR system from Hamilton Company. Several recovery standards were added prior to the first step in the extraction process for quality control (QC) purposes. To remove protein, dissociate small molecules

bound to protein or trapped in the precipitated protein matrix, and to recover chemically diverse metabolites, proteins were precipitated with methanol under vigorous shaking for 2 minutes (Glen Mills Geno/Grinder 2000) followed by centrifugation. The resulting extract was divided into 5 fractions: 2 for analysis by 2 separate reverse phase (RP)/UPLC-MS/MS methods with positive-ion mode ESI, 1 for analysis by RP/UPLC-MS/MS with negative-ion mode ESI, 1 for analysis by HILIC/UPLC-MS/MS with negative-ion mode ESI, and 1 sample was reserved for backup. Samples were placed briefly on a Zymark TurboVap to remove the organic solvent. The sample extracts were stored overnight under nitrogen before preparation for analysis.

QC. Several types of controls were analyzed in concert with the experimental samples: a pooled matrix sample generated by taking a small volume of each experimental sample (or alternatively, use of a pool of well-characterized human plasma) served as a technical replicate throughout the data set. Extracted water samples served as process blanks and a cocktail of QC standards that were carefully chosen not to interfere with the measurement of endogenous compounds were spiked into every analyzed sample and allowed instrument performance monitoring and aided chromatographic alignment. Instrument variability was determined by calculating the median relative standard deviation for the standards that were added to each sample prior to injection into the mass spectrometers. Overall process variability was determined by calculating the median relative standard deviation for all endogenous metabolites (i.e., noninstrument standards) present in 100% of the pooled matrix samples. Experimental samples were randomized across the platform run with QC samples spaced evenly among the injections.

UPLC-MS/MS. All methods utilized a Waters ACQUITY UPLC and a Thermo Fisher Scientific Q-Exactive high-resolution/accurate mass spectrometer interfaced with a heated electrospray ionization source and Orbitrap mass analyzer operated at a mass resolution setting of 35,000. The sample extract was dried and then reconstituted in solvents compatible to each of the 4 methods. Each reconstitution solvent contained a series of standards at fixed concentrations to ensure injection and chromatographic consistency. One aliquot was analyzed using acidic positive-ion conditions, chromatographically optimized for more hydrophilic compounds. In this method, the extract was gradient eluted from a C18 column (Waters UPLC BEH C18, 2.1 × 100 mm, 1.7 μm) using water and methanol, containing 0.05% perfluoropentanoic acid and 0.1% formic acid. Another aliquot was also analyzed using acidic positive-ion conditions; however, it was chromatographically optimized for more hydrophobic compounds. In this method, the extract was gradient eluted from the same aforementioned C18 column using methanol, acetonitrile, water, 0.05% perfluoropentanoic acid, 0.01% formic acid, and was operated at an overall higher organic content. Another aliquot was analyzed using basic negative-ion–optimized conditions using a separate dedicated C18 column. The basic extracts were gradient eluted from the column using methanol and water, however, with 6.5 mM ammonium bicarbonate (pH 8). The fourth aliquot was analyzed via negative ionization following elution from an HILIC column (Waters UPLC BEH Amide, 2.1 × 150 mm, 1.7 μm) using a gradient consisting of water and acetonitrile with 10 mM ammonium formate (pH 10.8). The MS analysis alternated between MS and data-dependent MS^n scans using dynamic exclusion. The scan range varied slighted between methods but covered 70–1000 mass-to-charge ratio (m/z). Raw data files are archived and extracted as described in the information to follow.

Bioinformatics. The informatics system consisted of 4 major components: (a) the LIMS, (b) the data extraction and peak-identification software, (c) data-processing tools for QC and compound identification, and (d) a collection of information interpretation and visualization tools for use by data analysts. The hardware and software foundations for these informatics components were the LAN backbone and a database server running Oracle 10.2.0.1 Enterprise Edition.

LIMS. The purpose of the Metabolon LIMS system was to enable fully auditable laboratory automation through a secure, easy-to-use, and highly specialized system. The scope of the Metabolon LIMS system encompasses sample accessioning, sample preparation and instrumental analysis, and reporting and advanced data analysis. All of the subsequent software systems are grounded in the LIMS data structures. It has been modified to leverage and interface with the in-house information extraction and data visualization systems, as well as third-party instrumentation and data analysis software.

Data extraction and compound identification. Raw data were extracted, peak-identified, and QC processed using Metabolon's hardware and software. These systems are built on a web-service platform utilizing Microsoft's.NET technologies, which run on high-performance application servers and fiber-channel storage arrays in clusters to provide active failover and load balancing. Compounds were identified by comparison to library entries of purified standards or recurrent unknown entities. Metabolon maintains a library based on authenticated standards that contain the retention time/index (RI), m/z, and chromatographic data

(including MS/MS spectral data) on all molecules present in the library. Furthermore, biochemical identifications are based on 3 criteria: retention index within a narrow RI window of the proposed identification, accurate mass match to the library ± 10 ppm, and the MS/MS forward and reverse scores between the experimental data and authentic standards. The MS/MS scores are based on a comparison of the ions present in the experimental spectrum to the ions present in the library spectrum. Although there may be similarities between these molecules based on one of these factors, the use of all 3 data points can be utilized to distinguish and differentiate biochemicals. More than 3300 commercially available purified standard compounds have been acquired and registered into LIMS for analysis on all platforms in order to determine their analytical characteristics. Additional mass spectral entries have been created for structurally unnamed biochemicals, which have been identified by virtue of their recurrent nature (both chromatographic and mass spectral). These compounds have the potential to be identified by future acquisition of a matching purified standard or by classical structural analysis.

Curation. A variety of curation procedures were carried out to ensure that a high-quality data set was made available for statistical analysis and data interpretation. The QC and curation processes were designed to ensure accurate and consistent identification of true chemical entities and to remove those representing system artifacts, missassignments, and background noise. Metabolon data analysts use proprietary visualization and interpretation software to confirm the consistency of peak identification among the various samples. Library matches for each compound were checked for each sample and corrected if necessary.

Metabolite quantification and data normalization. Peaks were quantified using AUC. For studies spanning multiple days, a data normalization step was performed to correct variation resulting from instrument inter-day tuning differences. Essentially, each compound was corrected in run-day blocks by registering the medians to equal 1.00 and normalizing each data point proportionately. For studies that did not require more than 1 day of analysis, no normalization was necessary, other than for purposes of data visualization. In certain instances, biochemical data may have been normalized to an additional factor (e.g., cell counts, total protein as determined by Bradford assay, osmolality, etc.) to account for differences in metabolite levels due to differences in the amount of material present in each sample.

RNA analysis

RNA was isolated from mouse tissues using TRIzol reagent (Invitrogen). cDNA was generated using iScript reverse transcription mix (Bio-Rad). Semiquantitative PCR was carried out on cDNA using gene-specific oligonucleotide primers. Real-time quantification was performed using SYBR Select Master Mix (Applied Biosystems) with the Applied Biosystems StepOnePlus Real-Time PCR system. Relative expression of genes of interest were normalized to that of β-actin and analyzed using the ΔΔCt method. Alternatively, expression levels of select miRNAs were determined from TRIzol-purified RNA samples using Quantigene Plex target-specific probes and capture beads, following the manufacturer's instructions (Affymetrix). The final data were obtained and analyzed via the Bioplex Magpix multiplex reader system (Bio-Rad).

Serum preparation

Serum was prepared from whole blood harvested at the time of euthanasia. Blood was placed in a 1.7-ml Eppendorf tube and allowed to clot at room temperature for 30 minutes. Blood samples were then centrifuged at 2000 rpm for 15 minutes, and serum was transferred to a clean tube and stored at –80°C.

Quantification of leptin and triglycerides

Leptin concentration was measured in the serum using the Mouse/Rat Leptin Quantikine ELISA Kit (R&D Systems). Serum triglycerides were measured using Triglycerides Reagent (Thermo Scientific). Liver tissue was digested overnight at room temperature in 5 M KOH, 50% ethanol solution (1-ml solution per 100-mg tissue). Lysates were briefly centrifuged to remove any particulate, and supernatant was used for the triglyceride assay.

Metabolic cage studies

Food intake, meal patterns, energy expenditure, and locomotor activity were monitored using a combined indirect calorimetry system (Labmaster, TSE Systems GmbH). Experimental animals were individually housed in a light- (12 hour on/12 hour off, 7 am to 7 pm) and temperature-controlled (21.5°C–22.5°C) environment and acclimated in the home cage for 5 days before data collection. Mice were then analyzed in the metabolic chambers for 10 days and were provided with food and water ad libitum. Mice were fed

a standard CD for the first 5 days, then switched to an HFD for the last 5 days. Oxygen consumption and carbon dioxide production were measured by indirect calorimetry to determine energy expenditure. Locomotor activity was measured using a multidimensional infrared light beam detection system. Continuous food and water intake were recorded using lid-mounted weighing sensors.

Statistics

All the values in the text and figures are presented as mean ± SEM, unless otherwise stated. Statistical significance was determined by 2-tailed Student's *t* test or ANOVA with Tukey's post hoc test where appropriate. *P* values of < 0.05 were considered significant.

Author contributions

BPW and WJK designed research studies. BPW, KSG, MAW, MCV, and AC conducted experiments and acquired data. BPW, MAW, KSG, JP, JKC, KD, and WJK analyzed data. BPW and WJK wrote the manuscript with assistance from KSG and JP.

Acknowledgments

WJK is the W.W. Smith Chair in Cardiovascular Medicine and the studies were supported in part by a predoctoral fellowship from the American Heart Association (to BPW) and NIH grants R37 HL061690, P01 HL075443, P01 HL134608, and a Merit Award from the American Heart Association 18MERIT33900036 (to WJK). The authors thank Philip Woodall for his assistance in formatting figures for the final manuscript.

Address correspondence to: Walter J. Koch, Department of Pharmacology, Center for Translational Medicine, Temple University, 3500 North Broad Street, 941 MERB, Philadelphia, Pennsylvania, 19140-4106, USA. Phone: 215.707.9820; Email: walter.koch@temple.edu.

1. Van Gaal LF, Mertens IL, De Block CE. Mechanisms linking obesity with cardiovascular disease. *Nature*. 2006;444(7121):875–880.
2. Kenchaiah S, Sesso HD, Gaziano JM. Body mass index and vigorous physical activity and the risk of heart failure among men. *Circulation*. 2009;119(1):44–52.
3. Crawford D, Jeffery RW, French SA. Can anyone successfully control their weight? Findings of a three year community-based study of men and women. *Int J Obes Relat Metab Disord*. 2000;24(9):1107–1110.
4. Boström P, et al. A PGC1-α-dependent myokine that drives brown-fat-like development of white fat and thermogenesis. *Nature*. 2012;481(7382):463–468.
5. Liu S, et al. A diurnal serum lipid integrates hepatic lipogenesis and peripheral fatty acid use. *Nature*. 2013;502(7472):550–554.
6. Shimizu N, et al. A muscle-liver-fat signalling axis is essential for central control of adaptive adipose remodelling. *Nat Commun*. 2015;6:6693.
7. Grueter CE, et al. A cardiac microRNA governs systemic energy homeostasis by regulation of MED13. *Cell*. 2012;149(3):671–683.
8. Baskin KK, et al. MED13-dependent signaling from the heart confers leanness by enhancing metabolism in adipose tissue and liver. *EMBO Mol Med*. 2014;6(12):1610–1621.
9. Iaccarino G, Tomhave ED, Lefkowitz RJ, Koch WJ. Reciprocal in vivo regulation of myocardial G protein-coupled receptor kinase expression by beta-adrenergic receptor stimulation and blockade. *Circulation*. 1998;98(17):1783–1789.
10. Petrofski JA, Koch WJ. The β-adrenergic receptor kinase in heart failure. *J Mol Cell Cardiol*. 2003;35(10):1167–1174.
11. Ungerer M, Böhm M, Elce JS, Erdmann E, Lohse MJ. Altered expression of β-adrenergic receptor kinase and β1-adrenergic receptors in the failing human heart. *Circulation*. 1993;87(2):454–463.
12. Koch WJ, et al. Cardiac function in mice overexpressing the β-adrenergic receptor kinase or a β ARK inhibitor. *Science*. 1995;268(5215):1350–1353.
13. Rockman HA, et al. Expression of a beta-adrenergic receptor kinase 1 inhibitor prevents the development of myocardial failure in gene-targeted mice. *Proc Natl Acad Sci U S A*. 1998;95(12):7000–7005.
14. Akhter SA, Eckhart AD, Rockman HA, Shotwell K, Lefkowitz RJ, Koch WJ. In vivo inhibition of elevated myocardial beta-adrenergic receptor kinase activity in hybrid transgenic mice restores normal beta-adrenergic signaling and function. *Circulation*. 1999;100(6):648–653.
15. Harding VB, Jones LR, Lefkowitz RJ, Koch WJ, Rockman HA. Cardiac beta ARK1 inhibition prolongs survival and augments β blocker therapy in a mouse model of severe heart failure. *Proc Natl Acad Sci U S A*. 2001;98(10):5809–5814.
16. Shah AS, et al. In vivo ventricular gene delivery of a beta-adrenergic receptor kinase inhibitor to the failing heart reverses cardiac dysfunction. *Circulation*. 2001;103(9):1311–1316.
17. Rengo G, et al. Myocardial adeno-associated virus serotype 6-βARKct gene therapy improves cardiac function and normalizes the neurohormonal axis in chronic heart failure. *Circulation*. 2009;119(1):89–98.
18. Raake PW, et al. AAV6.βARKct cardiac gene therapy ameliorates cardiac function and normalizes the catecholaminergic axis in a clinically relevant large animal heart failure model. *Eur Heart J*. 2013;34(19):1437–1447.
19. Chen M, et al. Prodeath signaling of G protein-coupled receptor kinase 2 in cardiac myocytes after ischemic stress occurs via extracellular signal-regulated kinase-dependent heat shock protein 90-mediated mitochondrial targeting. *Circ Res*.

2013;112(8):1121–1134.
20. Sato PY, et al. GRK2 compromises cardiomyocyte mitochondrial function by diminishing fatty acid-mediated oxygen consumption and increasing superoxide levels. *J Mol Cell Cardiol*. 2015;89(pt B):360–364.
21. Ciccarelli M, et al. G protein-coupled receptor kinase 2 activity impairs cardiac glucose uptake and promotes insulin resistance after myocardial ischemia. *Circulation*. 2011;123(18):1953–1962.
22. Garcia-Guerra L, et al. G protein-coupled receptor kinase 2 plays a relevant role in insulin resistance and obesity. *Diabetes*. 2010;59(10):2407–2417.
23. Vila-Bedmar R, et al. Reversal of diet-induced obesity and insulin resistance by inducible genetic ablation of GRK2. *Sci Signal*. 2015;8(386):ra73.
24. McCormack SE, et al. Circulating branched-chain amino acid concentrations are associated with obesity and future insulin resistance in children and adolescents. *Pediatr Obes*. 2013;8(1):52–61.
25. Pagano C, Rossato M, Vettor R. Endocannabinoids, adipose tissue and lipid metabolism. *J Neuroendocrinol*. 2008;20(suppl 1):124–129.
26. Vila-Bedmar R, et al. GRK2 contribution to the regulation of energy expenditure and brown fat function. *FASEB J*. 2012;26(8):3503–3514.
27. Rolfe DF, Brown GC. Cellular energy utilization and molecular origin of standard metabolic rate in mammals. *Physiol Rev*. 1997;77(3):731–758.
28. Sun K, Kusminski CM, Scherer PE. Adipose tissue remodeling and obesity. *J Clin Invest*. 2011;121(6):2094–2101.
29. Rosen ED, Spiegelman BM. What we talk about when we talk about fat. *Cell*. 2014;156(1–2):20–44.
30. Moon HS, et al. Leptin's role in lipodystrophic and nonlipodystrophic insulin-resistant and diabetic individuals. *Endocr Rev*. 2013;34(3):377–412.
31. Bordicchia M, et al. Cardiac natriuretic peptides act via p38 MAPK to induce the brown fat thermogenic program in mouse and human adipocytes. *J Clin Invest*. 2012;122(3):1022–1036.
32. Wu J, et al. Beige adipocytes are a distinct type of thermogenic fat cell in mouse and human. *Cell*. 2012;150(2):366–376.
33. Chen H, Simar D, Ting JH, Erkelens JR, Morris MJ. Leucine improves glucose and lipid status in offspring from obese dams, dependent on diet type, but not caloric intake. *J Neuroendocrinol*. 2012;24(10):1356–1364.
34. López N, Sánchez J, Picó C, Palou A, Serra F. Dietary l-leucine supplementation of lactating rats results in a tendency to increase lean/fat ratio associated to lower orexigenic neuropeptide expression in hypothalamus. *Peptides*. 2010;31(7):1361–1367.
35. Potier M, Darcel N, Tomé D. Protein, amino acids and the control of food intake. *Curr Opin Clin Nutr Metab Care*. 2009;12(1):54–58.
36. Pennetti V, Galante A, Zonta-Sgaramella L, Jayakar SD. Relation between obesity, insulinemia, and serum amino acid concentrations in a sample of Italian adults. *Clin Chem*. 1982;28(11):2219–2224.
37. Schauder P, Zavelberg D, Langer K, Herbertz L. Sex-specific differences in plasma branched-chain keto acid levels in obesity. *Am J Clin Nutr*. 1987;46(1):58–60.
38. Wang TJ, et al. Metabolite profiles and the risk of developing diabetes. *Nat Med*. 2011;17(4):448–453.
39. Estrada-Alcalde I, et al. Metabolic fate of branched-chain amino acids during adipogenesis, in adipocytes from obese mice and C2C12 myotubes. *J Cell Biochem*. 2017;118(4):808–818.
40. Halama A, et al. Metabolic switch during adipogenesis: from branched chain amino acid catabolism to lipid synthesis. *Arch Biochem Biophys*. 2016;589:93–107.
41. Green CR, et al. Branched-chain amino acid catabolism fuels adipocyte differentiation and lipogenesis. *Nat Chem Biol*. 2016;12(1):15–21.
42. Crown SB, Marze N, Antoniewicz MR. Catabolism of branched chain amino acids contributes significantly to synthesis of odd-chain and even-chain fatty acids in 3T3-L1 adipocytes. *PLoS One*. 2015;10(12):e0145850.
43. Shellhammer JP, et al. Amino acid metabolites that regulate G protein signaling during osmotic stress. *PLoS Genet*. 2017;13(5):e1006829.
44. Jang C, et al. A branched-chain amino acid metabolite drives vascular fatty acid transport and causes insulin resistance. *Nat Med*. 2016;22(4):421–426.
45. Sun H, et al. Catabolic defect of branched-chain amino acids promotes heart failure. *Circulation*. 2016;133(21):2038–2049.
46. Wang W, et al. Defective branched chain amino acid catabolism contributes to cardiac dysfunction and remodeling following myocardial infarction. *Am J Physiol Heart Circ Physiol*. 2016;311(5):H1160–H1169.
47. Di Marzo V, et al. Leptin-regulated endocannabinoids are involved in maintaining food intake. *Nature*. 2001;410(6830):822–825.
48. Engeli S, et al. Activation of the peripheral endocannabinoid system in human obesity. *Diabetes*. 2005;54(10):2838–2843.
49. Osei-Hyiaman D, et al. Endocannabinoid activation at hepatic CB1 receptors stimulates fatty acid synthesis and contributes to diet-induced obesity. *J Clin Invest*. 2005;115(5):1298–1305.
50. Ravinet Trillou C, et al. Anti-obesity effect of SR141716, a CB1 receptor antagonist, in diet-induced obese mice. *Am J Physiol Regul Integr Comp Physiol*. 2003;284(2):R345–R353.
51. Liu J, et al. Multiple pathways involved in the biosynthesis of anandamide. *Neuropharmacology*. 2008;54(1):1–7.
52. Pacher P, Mukhopadhyay P, Mohanraj R, Godlewski G, Bátkai S, Kunos G. Modulation of the endocannabinoid system in cardiovascular disease: therapeutic potential and limitations. *Hypertension*. 2008;52(4):601–607.